ADVANCED OPTICAL MATERIALS
www.advopticalmat.de

Optimized Two-Color Single-Molecule Tracking of Fast-Diffusing Membrane Receptors

Chiara Schirripa Spagnolo, Aldo Moscardini, Rosy Amodeo, Fabio Beltram, and Stefano Luin**

Single particle tracking (SPT) combined with total internal reflection fluorescence microscopy (TIRFm) is an outstanding approach to decipher mechanisms on the cell membrane at the nanoscale. Multicolor configurations, needed to investigate interactions, are still hindered by several challenges. This work systematically and quantitatively analyzes the impact of necessary elements of SPT-TIRFm setups on the signal-to-noise ratio (SNR), which must be optimized especially in dynamic studies needing minimally invasive dyes for biomolecule labeling. Autofluorescence originating from commonly used optical glass results in the dominant limiting factor in TIRFm, and a cover glass material is tested yielding significant SNR improvements in multichannel TIRFm. Moreover, methodologies are optimized for reducing fluorophore photobleaching in multicolor implementations requiring simultaneous stabilization of multiple dyes. The developed strategies are applied to the fast p75^{NTR} receptors labeled by two fluorophores on the membrane of living cells, achieving reliable, simultaneous two-color SPT, contrary to configurations using standard cover glasses. This work highlights the importance of optical materials suitable for microscopy and with reduced autofluorescence for increasing sensitivity toward ultimate spatiotemporal resolutions. In particular, the present protocols can pave the way for multicolor super-resolved localization and tracking of single molecules by TIRFm, greatly expanding the potential of SPT.

1. Introduction

Total internal reflection fluorescence microscopy (TIRFm) is a powerful technique for visualizing key biological events occurring on the cell membrane with outstanding signal-to-noise ratio and spatial resolution.[1–3] TIRFm can reach the single-molecule level and, especially when combined with single-particle tracking (SPT), can yield an accurate description of the spatio-temporal organization of the cell membrane environment and provide much information on its structure and functioning.[4–6] SPT provides the exceptional ability to observe directly each molecule at work in a living system. So far, the major reported developments are in the context of single-color SPT, where single particles of a unique molecular kind are labelled and tracked over time. These studies provided many new insights into molecule dynamics and homo-interactions, revealing the strong correlation between these and biological mechanisms.[7–9]

Multicolor extensions of TIRFm-based SPT allow the visualization of multiple kinds of molecules and enable the quantitative study, at the single-molecule level, of hetero-interactions on the cell membrane, e.g. interaction of different receptors with one another or of receptors with their ligands. Indeed, signal transduction is typically determined by complex interplays of different molecules and deciphering such mechanisms requires the simultaneous observation of different moieties. However, multicolor SPT applications are still limited and are hindered by several experimental difficulties. From the point of view of the microscopy setup, the simplest implementations are based on the use of Quantum Dots (Qdots), owing to their high brightness and photostability and the possibility to use a single excitation.[10–12] However, an important drawback of Qdots is their relatively large size, with a typical reported diameter of 10–50 nm, compared to 1–2 nm for organic dyes.[10,13] Indeed, some studies revealed the impact of steric hindrance and a slowed dynamics due to Qdot labelling.[7,14] Moreover, the presence of multiple functionalizable moieties on Qdots prevents the simultaneous control of stoichiometry and efficiency, contrary to organic dyes.[11,15] For these reasons, we chose to use small

C. Schirripa Spagnolo, A. Moscardini, R. Amodeo[+], F. Beltram, S. Luin
NEST Laboratory
Scuola Normale Superiore
piazza San Silvestro 12, Pisa I-56127, Italy
E-mail: chiara.schirripaspagnolo@sns.it; s.luin@sns.it
F. Beltram, S. Luin
NEST Laboratory
Istituto Nanoscienze-CNR
piazza San Silvestro 12, Pisa I-56127, Italy

The ORCID identification number(s) for the author(s) of this article can be found under https://doi.org/10.1002/adom.202302012

[+]Present address: Department of Biomedical Sciences, Humanitas University, Via Rita Levi Montalcini 4, Pieve Emanuele, Milan 20072, Italy

DOI: 10.1002/adom.202302012

and minimally invasive organic dyes, selecting the brightest ones among those commercially available.

eHere we investigate the experimental challenges related to two-color single-particle tracking using these labels, a technique that we implemented using a commercial TIRFm setup by adding a laser combiner before the optical fiber coupled to the setup and a DualView to acquire two emission channels simultaneously on a single fast electron-multiplier charge-coupled device (EM-CCD). In the past, multicolor single molecule imaging, spectroscopy and/or tracking have been performed for immobilized molecules or for relatively slow diffusing molecules (diffusivities of the order of 10^{-2} μm^2 s^{-1} or below), however limitations in the analysis were already noticed due to low signal-to-noise ratios.[16]

We analyze the two critical issues related to the choice of these labels: low signal-to-noise ratio and photobleaching. The former is caused by the relatively low brightness of the dyes and by the background that can be significant, especially with the multiple excitations required for these dyes. We show that several background sources exist among the necessary elements of a TIRFm system, and their unwanted emission becomes more severe in multicolor implementations. Limited reports exist on these effects: there are some studies of autofluorescence from optical glasses or biomolecules but they are few and mainly concern excitation in the UV range.[17–21] Even if the disturbing autofluorescence background from optical components have sometimes been noticed in the literature regarding different kind of optical devices,[22–25] this issue was not explored thoroughly, e.g. by investigating quantitative effects in specific applications. An additional difficulty is that autofluorescence characteristics are usually not considered or not described by manufactures of optical glasses. Therefore, there is a need for studies that highlight the impact of this kind of phenomenon and propose improving solutions, in particular suitable for microscopy. For instance, here we observe a strong impact of the background arising from standard borosilicate cover glasses, and we describe the use of an optical material that, once the setup is optimized for correcting spherical and/or chromatic aberrations, significantly improves the final signal-to-noise ratio for the case of dyes in a two-color configuration.

We also deal with photobleaching. This is a complex phenomenon caused by the combination of different mechanisms; several strategies for reducing its impact were proposed, but the efficacy of a possible antibleaching solution strongly depends on the considered dye.[26,27] Therefore, reducing photobleaching in multicolor studies is even more challenging because a common solution must be found for different dyes. We investigated the effects of different possible antibleaching reagents (namely Trolox, ascorbic acid and n-propyl gallate) on the dyes of interest, finding the best combination and concentrations of reagents to obtain an effective strategy to simultaneously reduce photobleaching for both the selected dyes.

Finally, we show that the approach here presented allows performing two-color SPT experiments in living cells on fast p75^{NTR} receptors labelled with two different organic dyes, obtaining reliable tracking results in both channels. Through experiments and simulations, we demonstrate that using standard cover glasses instead of the newly introduced one produces instead altered results.

2. Results

2.1. Effects of Background on the Signal-to-Noise Ratio (SNR) of Single Molecules

We measured the background in a "standard" TIRFm system without any fluorescent sample, but with all the other essential elements, i.e., immersion oil (Leica type F), glass coverslip bottom of the dishes (WillCo-dish Glass Bottom dishes), water medium (**Figure 1**A; we used this as a reference system for normalizing most of the measurements reported below). This background depends strongly on excitation- and detection-band combinations, as observed in typical configurations used for single-molecule fluorescence (Figure 1A), and this strongly impacts on the SNR of dyes, especially in single-molecule measurements. We measured the SNR of the dyes Atto 565 and Abberior STAR 635p: they have identical brightness, comparable extinction coefficient and quantum yield (Table S1, Supporting Information), but the SNR of the latter was found to be significantly lower due to the different background associated with the individual excitation and detection wavelengths (Figure 1B). We observed this behavior both on immobile dyes adherent to the thin glass bottom of Petri dishes for microscopy (called "cover glass" from here on for simplicity) and on dyes labelling the neurotrophic TrkA receptors that diffused on the membrane of living cells. For each dye, the SNR was higher when the dyes adhered to the coverslip than when they labelled TrkA receptors; this is expected, and potentially caused by a combination of effects: an additional biological source of autofluorescence, a lower signal caused by the distance of the membrane from the glass-water interface, and especially the impact of receptors movement. Indeed, diffusion causes a degradation of the SNR, as we also observed by comparing the SNR of two receptors having different diffusivities, TrkA and P75^{NTR} (Figure S1, Supporting Information). Hence experiments on moving molecules in living cells, such as SPT, are the ones most affected by the typically low SNR, and it is crucial to investigate strategies for its improvement.

Figure 1A suggests that these effects may become even more relevant in a multicolor setup because of the high background in the far-red region upon excitation with a shorter wavelength such as 488 or 565 nm. We observed that a relevant contribution to this background is due to the emission of optical glass, in particular of the cover glass. Indeed, we measured the emission of a typical one (Schott D263M) with a 473 nm excitation in a microRaman system and we observed higher emission in the longer-wavelength portion of the spectrum (Figure 1C).

We then compared three possible implementations of a two-color TIRFm system with the following three dye pairs (Figure 1D, see also Experimental Section): i) 488-excitation, green dye paired with a 561-excitation, orange dye; ii) 561-excitation, orange dye paired with a 635-excitation red dye; iii) 488-excitation, green dye paired with a 635-excitation red dye. We selected the dyes (Alexa 488, Atto 565 and Abberior STAR 635p) among the ones already used in single-molecule applications with the highest brightness for the corresponding channel.[7,11,28]

We observed that the 488–565 couple was the one with the most homogeneous properties in the two channels; the 488–635 couple was the less advantageous; the 565–635 couple had a very different SNR in the two channels, with the first channel

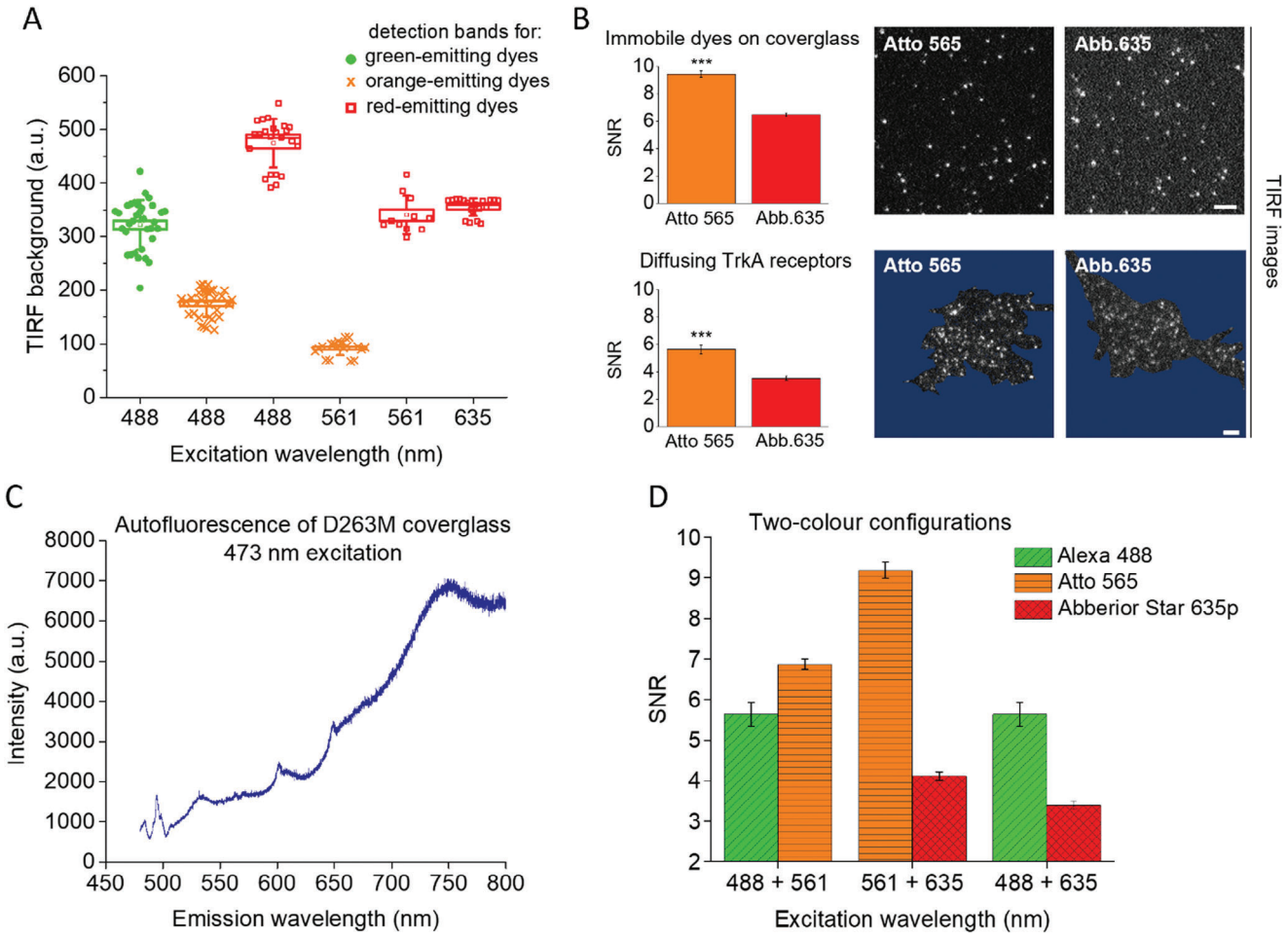

Figure 1. Background behavior and its effects in single-molecule TIRF microscopy A) Background detected in TIRFm with different combinations of excitation and detection bands with standard glass (D263M)-bottom Petri dishes (at fixed excitation power and EM-CCD parameters). Bands and parameters are detailed in Experimental Section and Supplementary Methods sections. Box: standard error of the mean (SEM); whisker: SD; dots: individual fields of view, from 5 independent repetitions. B) Signal-to-noise ratio (SNR) measured in single-molecule TIRFm for the two dyes Atto 565 and Abberior STAR 635p (Abb.635) having comparable brightness (see Table S1, Supporting Information) but excitation and detection bands corresponding to different background levels. Results reported for dyes adherent to cover glass (top) and labelling moving TrkA receptors on the membrane of adherent live SH-SY5Y cells (bottom), with corresponding representative TIRF images on the right (the region outside the basal cell membrane is colored uniformly in blue for images on the bottom). The images are shown in the same fixed grayscale. Data are mean ± SEM. Dyes on cover glass: 7 movies in different fields of view from 2 independent repetitions; dyes labelling TrkA receptors: 16 movies in different fields of view from 3 independent repetitions. Intensity signal mediated in space and time on a total of 2000–20000 spots for each movie. ***$P < 0.001$, Student's t-test. Scale bar: 3 µm C) Typical emission spectrum for D263M cover glass using excitation at 473 nm. D) Evaluation of SNR in three two-channel configurations (estimated from single-channel measurements as described in the Experimental Section), using dyes adherent to cover glass. Data are mean ± SEM, obtained from 4–9 movies in different fields of view from 2 independent repetitions; intensity signals mediated on 2000–13000 spots for each movie.

having more-than-double SNR. The choice of the best configuration may depend on the application of interest, e.g. on the diffusivity of the molecules imaged in the two channels. However, the 565–635 and 488–635 couples showed a considerable limit in the far-red channel owing to the background detected in that region.

From these preliminary observations we concluded that i) the behavior of the background caused by the necessary elements in a TIRFm system strongly influences the SNR for single molecules; ii) in the choice of channels for single and multi-color studies it is important to consider the different background contributions associated with the various excitation-detection pairs rather than to consider only the dye brightness; iii) glass emission can be a limiting factor for multi-color applications.

2.2. N-PK51 Optical Glass as Cover Glass Material for TIRFm

Due to the high impact of the cover glass fluorescence on the background, especially for multicolor applications, we compared the emission intensity of different cover glasses at different excitations and emission bands combinations (**Figure 2**A). Schott D263M is a borosilicate glass used to make cover glasses of different brands and is incorporated in glass-bottom dishes from many companies (such as Willco Dishes, Ibidi, Azer Scientific). We identified a few brands that use different kinds of borosilicate glasses for the bottom of their dishes, e.g. MatTek dish and FluoroDish, even if these companies do not supply additional information on the used material. We also investigated the

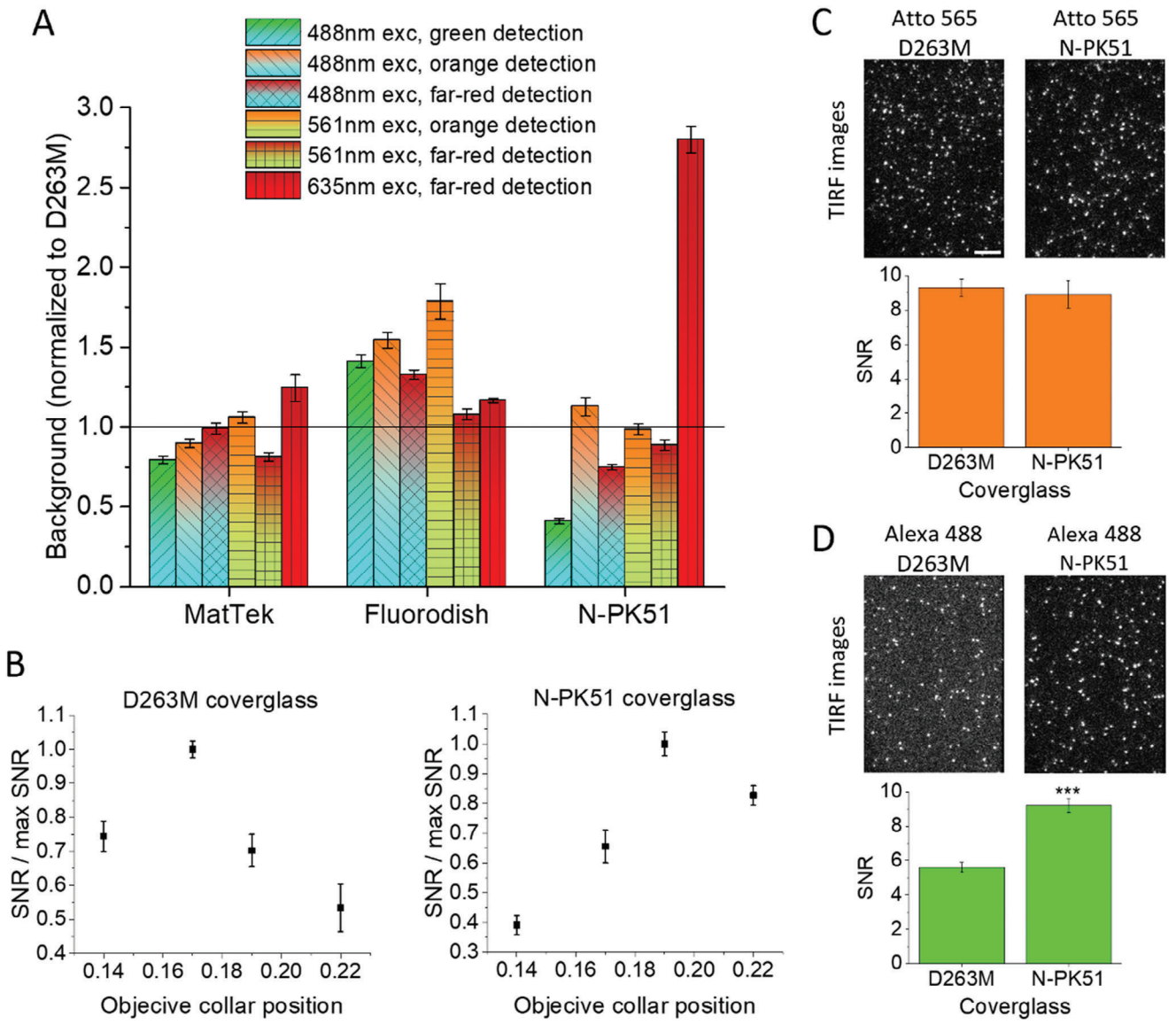

Figure 2. Cover glasses comparison and use of N-PK51 glass for single-molecule TIRF imaging. A) Ratio between the background detected using different cover glass kinds and using D263M cover glass. Bar color gradients illustrate excitation (bottom) and detection (top) wavelengths. Data are mean ± standard error of the mean (SEM), obtained from 8–23 fields of view from 2 independent repetitions. B) SNR of single molecules of Atto 565 adhered on D263M (left) and N-PK51 (right) cover glasses at different objective collar positions, normalized to the maximum observed SNR. Measurements were performed at 37 °C. Data are mean ± SEM, obtained from 5 movies in different fields of view from 2 independent repetitions, with 2000–20000 spots analyzed in each movie. C) Top: representative TIRF images of single molecules of Atto 565 adhered on D263M (left) and N-PK51 (right) cover glass, shown in the same grayscale. Bottom: corresponding SNR. D) Top: representative TIRF images of single molecules of Alexa 488 adhered on D263M (left) and N-PK51 (right) cover glass, shown in the same grayscale. Bottom: corresponding SNR. Images in C) and D) were acquired separately in single-channel configurations. Data are mean ± SEM, obtained from 10 movies in different fields of view from 2 independent repetitions, with 2000–20000 spots analyzed in each movie. ***$P < 0.001$, Student's t-test. Scale bar: 5 µm; images reported with the same grayscale.

possibility of using different non-standard materials, considering however that TIRFm systems, especially the objective-based commercial ones, place severe limitations on the optical properties of the cover glass. Indeed, the setups are designed to be used with a cover glass with a thickness of 0.17 mm and a refractive index of 1.52 (at ≈550 nm). We considered Schott N-PK51 glass as a possible candidate, because of its refraction index and considering the few published data on glasses fluorescence (see Note S1 and Figure S2, Supporting Information), and obtained custom cover glasses made from this material (specifications in Tables S2 and S3, Supporting Information). In the autofluorescence comparisons between MatTek, FluoroDish and N-PK51, we found the biggest improvement over the D263M case using N-PK51, especially considering the green-region emission under excitation at 488 nm, which was reduced to 40% compared to D263M. Instead, on N-PK51, the emission detected in the far-red under red excitation was 2.4 times higher compared to D263M (see also Supplementary discussion),

more than compensating the small improvement in the far-red emission upon blue excitation in a hypothetical 488–635 couple for simultaneous two-color applications. We did not find a material able to significantly improve the SNR of the 635-channel, which was relatively low in two-color configurations, as shown in Figure 1D for D263M; therefore, in the following we will mostly show results on dyes with excitations at 488 and 561 nm.

From the point of view of autofluorescence, N-PK51 seems a promising material; in the following and in the next section, we will show that the small changes in refractive index and its dispersion with respect to the "standard" D263M (Table S3, Supporting Information) did not hinder its use as a cover glass. First, we did not observe any shift or additional visible inhomogeneity in the illuminated area (while, e.g., using a fused silica or quartz cover glass only half field results illuminated). Considering possible (spherical) aberrations, we exploited the correction collar present in most modern TIRFm-objectives which can compensate for small variations in cover glass thickness (typically up to ≈50 micrometers) or variations in refractive indexes caused, e.g., by temperature changes. We searched for the best position of the objective correction collar using the standard D263M cover glasses and the N-PK51 custom cover glasses. Figure 2B reports the measured SNR of Atto 565 as a function of collar position at 37 °C; in this figure, we report data collected using Leica and Nikon immersion oils for D263M and N-PK51 respectively, since these combinations was found to be the best compromise considering also chromatic aberration (see Section 2.3), but analogous results were found also using different oils (Figure S3, Supporting Information). As expected, the optimal position for D263M is that for 0.17 thickness, while there is a small shift for N-PK51 due to the small difference in refractive index. The change in SNR seems caused mostly by a difference in the intensity of the single molecule spots; we would expect a broadening of the point spread function (PSF) for situations different from the optical one, but these resulted too small to be detected in our experiments performed on single Atto 565 molecules (Figure S4, Supporting Information): the fitted PSF width does not change significantly with the different collar positions. The SNR for Atto 565 dye with optimal collar positions was comparable between D263M and N-PK51 (Figure 2C; Figure S3, Supporting Information); considering also that we measured a similar autofluorescence of the two materials in the orange-dye emission band (Figure 2A), this means that we can correct the aberration due to the slight refractive index mismatch by using the correction collar.

When comparing the SNR for 488 dyes, we observed a significant improvement using the N-PK51 cover glass (Figure 2D). Thus, a first advantage of this material relates to single-color applications where 488 dyes are preferred, and the final obtainable SNR of these dyes, typically having lower brightness, is comparable to that achievable with brighter dyes emitting at different wavelengths (Table S1, Supporting Information). Thanks to this significant improvement in the 488-dye channel, the material promises a better two-color performance compared to standard D263M using 488 and 565 channels.

2.3. Two-Color Single-Molecule Imaging: Immersion Oil

To investigate the performance of the N-PK51 glass in a simultaneous two-color setup, we employed a single-fiber excitation setup. In order to minimize chromatic aberration, and in particular the focal distance between the two channels, we tested different immersion oils, finding that they influence these chromatic aberrations (**Figure 3**A–C). We found different behaviors for N-PK51 and D263M materials (Figure 3A–C), which could stem from a difference in the Abbe number (Table S2, Supporting Information). All the immersion oils have the same nominal refractive index (Table S4, Supporting Information); indeed, we found the same optimal collar position and negligible differences in maximum SNRs comparing different oils (Figure S3, Supporting Information). They have some differences in their Abbe number (Table S4, Supporting Information) but, interestingly, we found different degrees of chromatic aberration even among oils with the same theoretical Abbe number (e.g., Nikon and Olympus oils with the D263M cover glass, Figure 3B).

We also compared the background detected in the system with simultaneous two-color excitation using various immersion oils developed for fluorescence microscopy. We performed the measurements on D263M cover glass and, based on our results, we excluded Cargille LDF, while the others showed comparable behaviors (Figure 3D). The Nikon oil is the one minimizing chromatic aberration using N-PK51 cover glasses in our system and Figure S5 (Supporting Information) shows that the contribution of oil autofluorescence is similar for all considered oils (excluding Cargille LDF). For these reasons, from now on we will use the Nikon oil with N-PK51 cover glasses.

With the identified best conditions in our system (collar position and immersion oil) for each cover glass, we measured the SNR in a real two-color TIRFm configuration with simultaneous double excitation and detection. We report in Figure 3E the SNR averaged on time series, and we checked that there were no significant temporal trends during the acquisitions (Figure S6, Supporting Information). On dyes adhered to the cover glasses, we found no significant differences for the 565-dye; instead, we found a significant improvement for the 488-dye using the N-PK51 cover glass (Figure 3E).

2.4. Cell Autofluorescence

Another known source of autofluorescence is the cell itself.[29] We measured cellular autofluorescence with the chosen excitation-detection couples for the two-color configuration based on 488 and 565 dyes, i.e., 488 nm excitation with green and orange detection and 561 nm excitation with orange detection. We also performed the measurement using 635 nm excitation with far-red detection in order to have a comparison with this configuration, typically used in single-channel experiments. **Figure 4** reports the results obtained from measurements at different TIRFm penetration depths, and in particular Figure 4 A reports the average fluorescence intensity measured in areas with cells normalized to the one arising from zones without cells (and therefore, due to the autofluorescence of glass and eventually immersion oil and

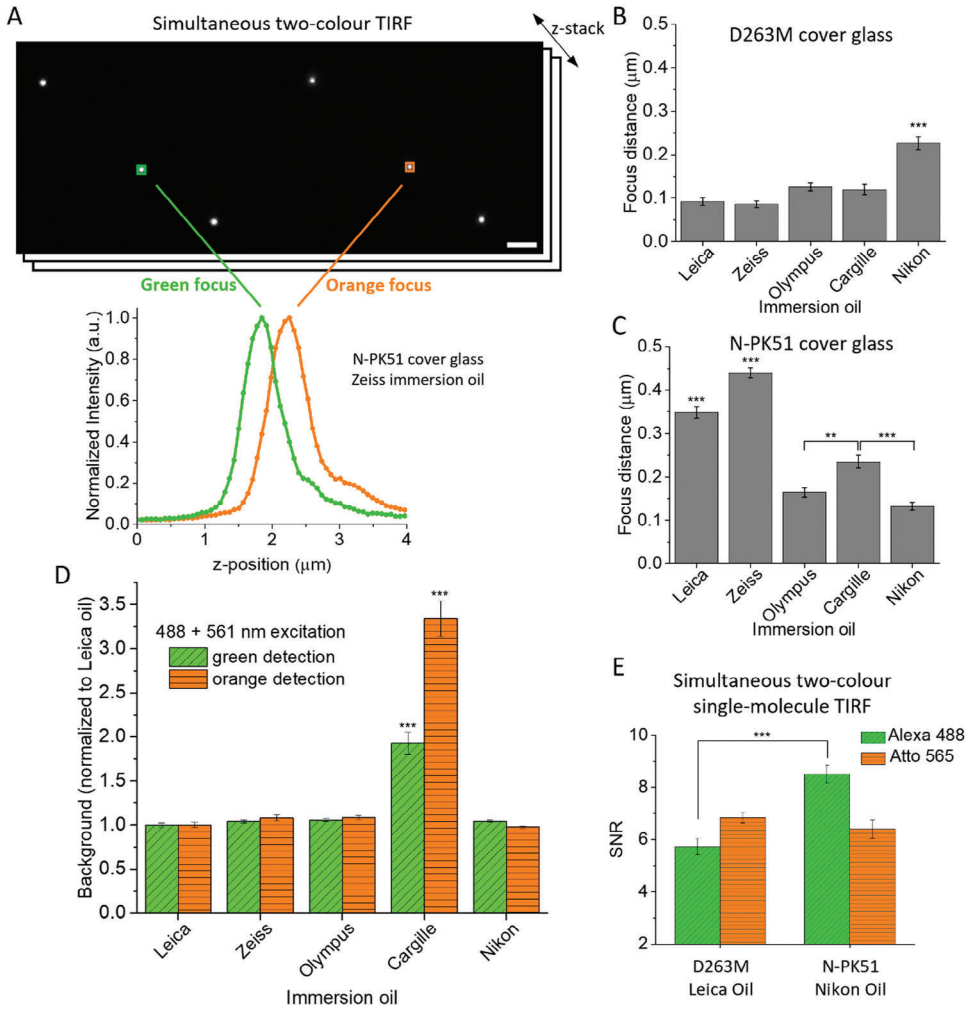

Figure 3. Effects of immersion oil on chromatic aberrations and background. A) Chromatic aberration is evident from the graphs of intensity z-profiles of single fluorescent beads able to emit in different wavelength bands, imaged simultaneously in the two channels (green and orange graphs for emissions in the green and orange channels). On top, example of images taken at 2 µm. Scale bar: 3 µm. B) Distances between the focus z-positions (the one corresponding to the maximum intensities in panel A) of the two channels using different immersion oils and D263M cover glass. C) Same as (B) with N-PK51 cover glass. Data are mean ± standard error of the mean (SEM), obtained from profiles of 30 beads in each condition. ***$P < 0.001$, **$P < 0.01$, 1-way ANOVA, Bonferroni multiple comparisons. D) Background detected in TIRFm under simultaneous 488 + 565 nm excitation using different immersion oils (measurements performed with D263M cover glass, see also Figure S5, Supporting Information). Data are mean ± SEM, obtained from 7 different fields of view. Data are normalized to the result obtained with Leica oil for each channel. ***$P < 0.001$, 1-way ANOVA, Bonferroni multiple comparisons. Tests performed separately on the green and orange results sets. E) SNR for single molecules of Alexa 488 and Atto 565 adherent on the cover glass in a TIRFm configuration with simultaneous excitation and detection. Measurements were performed using the immersion oil that minimizes chromatic aberration for each coverglass: Leica oil for D263M cover glass (left) and Nikon oil for N-PK51 cover glass (right). Data are mean ± SEM, obtained from 5 movies in different fields of view, with 2000–20000 spots analyzed in each movie. ***$P < 0.001$, Student's t-test. Tests performed separately on the green and orange couples of measurements.

medium). As shown in the example reported in Figure 4B, cell fluorescence is mostly inhomogeneous and seems to arise from structures inside the cell, since it is higher at deeper penetration; this is coherent with the observation reported in the literature that cell fluorescence arises from intracellular components and it is most intense in discrete cytoplasmic vesicles.[29] As shown in Figure 4, the additional contribution of cell autofluorescence to the total background is typically not higher than the one observed in zones without cells; as expected, it is higher when excited at 488 nm than at 565 and 635 nm and, in the first case, it is similar in the green and orange emission channel. However, this is clear only at the longest light penetration depths, while for penetrations of 130 nm and lower, the contribution to background due to cell autofluorescence did not exceed 5% of the measured background even in the case of excitation at 488 nm, and it reached 2% for 100-nm penetration-depth, the typical one used for single-molecule imaging and tracking of cell-surface proteins.[30] The contribution of cell autofluorescence on the total background is significantly lower in the other two channels at this penetration depth as well, as demonstrated from the data in Figure 4A and better compared in Figure S7 (Supporting Information). In this figure it is also clearer that, with excitation at 100-nm

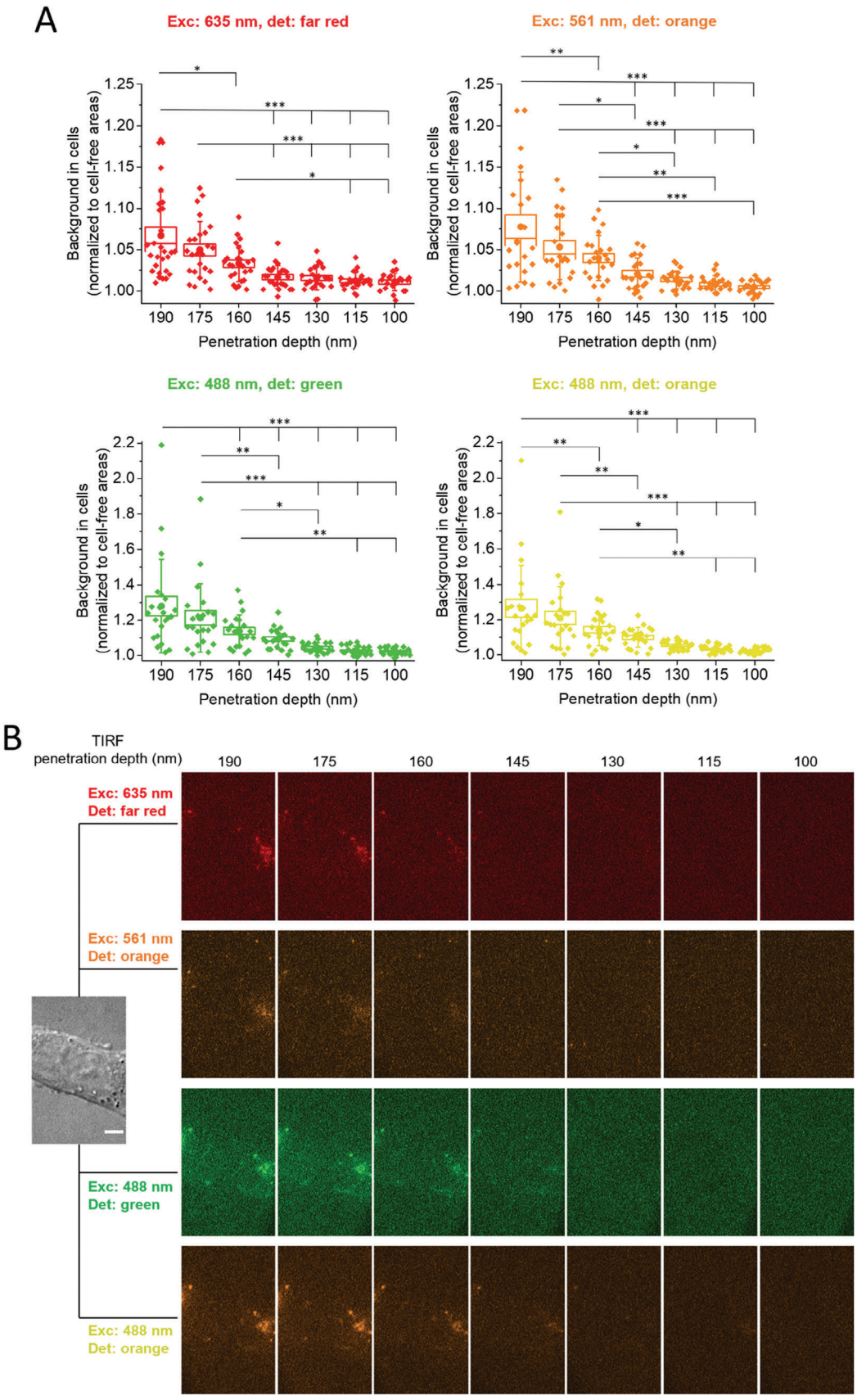

penetration-depth at 635 nm with far-red detection and at 561 nm with orange detection, cells produce a background equal to 1.01 times the background detected in cell-free areas, while this quantity becomes 1.02 under excitation at 488 nm. This shows that, in the described case, the contribution of cell autofluorescence to the total background is negligible (≈1 and 2%), and that the increase in cell background contribution under 488 nm excitation is so minimal (1%) compared to the 635-channel, that we can confirm the choice of 488 and 565 channels.

2.5. Cell Medium Autofluorescence

Highly sensitive live-cell imaging calls also for the optimization of the cell-imaging medium. Indeed, traditional growth media typically induce autofluorescence signals that negatively impact the available SNR.[31] On the other side, imaging in balanced salt solutions without nutrients lead to poor cell health. Typically, the highest growth media emissions are induced by UV, violet (405 nm) or blue (488 nm) excitation, while absorbance above 600 nm is usually not significant.[31] A correlation between the vitamin content and media autofluorescence induced at excitations lower than 500 nm, including 488 nm was observed.[31,32] Low-fluorescence media formulations with optimized vitamins (e.g., riboflavin) were developed.[31,32] Among these, FluoroBrite DMEM was tested for long-term live-cell imaging and cell culture maintenance, even on vitamin-sensitive and nutrient-sensitive cell lines.[32]

In order to monitor the impact of cell media fluorescence, we compared the background emissions detected using saline buffers and the cell media RPMI, DMEM, DMEM/F12, FluoroBrite DMEM (all red-phenol-free). We observed significantly higher emission with 488 nm excitation from cell media RPMI, DMEM and DMEM/F12 with respect to PBS, in both green and orange regions (**Figure 5**). An element likely involved in this behavior is riboflavin since, under excitation at 488 nm, it emits between 500 and 650 (green/red) with a main peak in the green region at 535 nm.[33,34] Riboflavin is present in all three media; however, in DMEM it has a concentration of 0.4 mg/L, twice the value in the other two media (information available from the producer Thermofisher Scientific). This may explain the higher fluorescence detected with DMEM. Importantly, FluoroBrite DMEM fluorescence was not significantly different from PBS or from a solution of HEPES and salts in our tests (Figure 5; see Supplementary Methods for the detailed composition); moreover, we did not find any significant difference when adding some common supplements (Figure S8, Supporting Information).

2.6. Photostability Improvement for Two-Color Imaging of 488 and 565 Channels

After SNR optimization, we addressed photobleaching, a severe limitation for single molecule tracking especially when using organic dyes.[12] First, we compared the photobleaching lifetimes (PBLTs) of the most popular 488-dyes used in single-molecule imaging (i.e., Alexa 488, Atto 488, Abberior STAR 488) (Figure S9A, Supporting Information). We found significant differences, with Atto 488 being the most photostable. The brightness of Atto 488 is the highest as well (even if not by much; see Table S1, Supporting Information). Atto 565 was more photostable than the 488-dyes in our experimental conditions. Therefore, we selected Atto 488 and Atto 565 for the following measurements (Figure S9B, Supporting Information).

Various antifading agents were proposed for use in cell cultures, among which ascorbic acid (AA), n-propyl gallate (NPG), and Trolox (TX).[35,36] Higher efficacy of TX was reported, in some cases, when it was partially oxidized to form a small percentage of Trolox-quinone (TQ), acting therefore as a reducing-plus-oxidizing system (ROXS).[27,36] Since this effect depends on the considered dyes,[27] we looked for the optimal TQ percentage for the two dyes of interest. We first monitored Trolox oxidation under UV illumination[36] (Figure S10A,B, Supporting Information). In absorbance measurements of a fresh Trolox solution, we observed its characteristic absorbance peak at ≈290 nm; using different UV-excitation times, we observed the formation of a new peak at ≈270 nm due to the TQ with the expected isosbestic point at ≈285 nm. [36] For each UV illumination time, we extracted the corresponding percentage of formed quinone (Figure S10B, Supporting Information) and the PBLT of the two dyes observed in TIRFm measurements in the presence of the corresponding solution (Figure S10C, Supporting Information). In both cases, we observed that the best condition is the use of Trolox without oxidation, with an approximately linear decrease in PBLT as the quinone concentration increased. The decrease of photobleaching lifetime cannot be ascribed simply to a lower effect of Trolox due to its lower concentration, rather it seems that the TQ increases the photobleaching of the considered dyes. It was reported that the ROXS approach tends to give greater improvements for far-red-emitting dyes (such as Atto 655, Atto 647N, Cy5[36,37]) and little or no improvements on fluorophores excited at shorter wavelengths.[38,39] This was attributed to an increasing influence of higher-excited states in photobleaching pathways over the triplet state (suppressed by ROXS) as the excitation energy increases. Furthermore, higher energy excitations may enhance the creation and impact of reactive oxygen species (ROS). TX was used in non-oxidized form in all the following measurements.

The best concentrations of TX, AA and NPG as antibleaching agents are not univocally determined in the literature. TX was used at 1–2 mM,[27,37,40] AA was used in mM concentrations (1–10 mM) but also in the μM range, [35,39,41] NPG was used at concentrations ranging from few μM to 10 mM.[35,42] Therefore, we measured the effect of different concentrations of the three reagents separately on the two dyes Atto 565 and Atto 488 (**Figure 6**; Figure S9B, Supporting Information). We extracted the

Figure 4. Cell autofluorescence in TIRFm. A) Cell autofluorescence measured on SK-N-BE(2) cells in WillCo petri dishes for different excitations (Exc) and detections (det) wavelengths, using different TIRF penetration depths. The y axis reports the ratio between the average total fluorescence intensity measured inside cells and the one measured in cell-free areas (see also Supplementary Methods). *$P < 0.05$, **$P < 0.01$,***$P < 0.001$, 1-way ANOVA, repeated measurements, Tukey multiple comparisons. Box: standard error of the mean (SEM), whiskers: standard deviation, spots: single cells from two independent repetitions. B) Representative images of the experiment: a cell (DIC image on the left) is visualized with the different excitation-detection combinations at different TIRF penetration depths (scale bar: 5 μM).

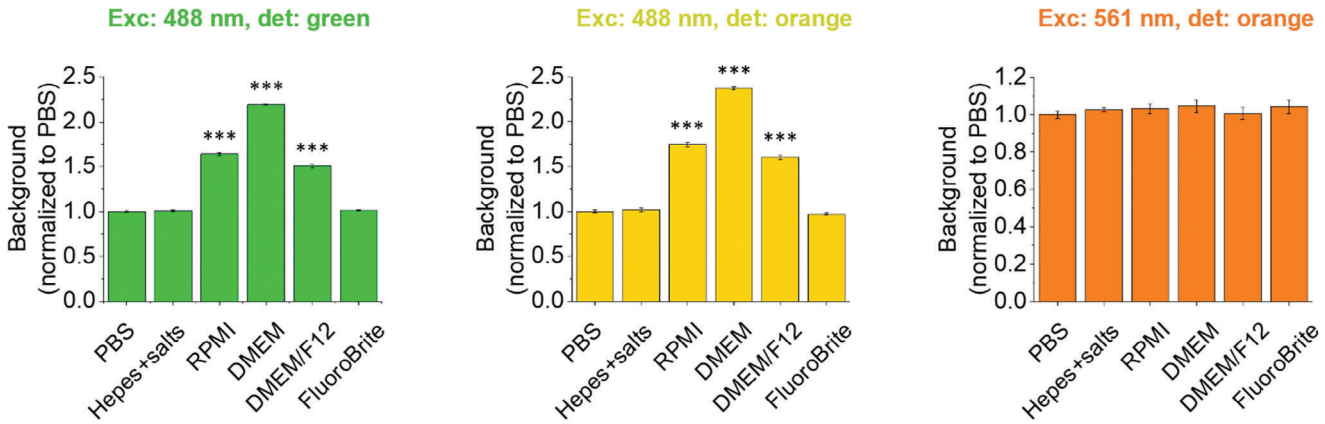

Figure 5. Background detected with different cell media. Background detected in TIRFm using different cell media. Results are mean ± standard error of the mean (SEM), obtained from 6–16 different fields of view from two independent repetitions. ***$P < 0.001$, 1-way ANOVA, Bonferroni multiple comparisons.

intensity-decay profiles that were fitted by an exponential function to extract the PBLT (see Supplementary Methods). We found that each of the reagents had a positive effect on the PBLT for both dyes. However, there are several differences in the observed effects. Comparing the plateau PBLTs, TX was the most effective additive for Atto 488, while AA and NPG had similar effects; NPG was the most effective and AA was the least effective on Atto 565. Moreover, for Atto 488, TX and AA had concentrations of a few mM at the plateau, while NPG required just a few μM. Similarly, Aitken et al. noted that 100 μM NPG (used in their work at lower concentration just due to its lower solubility) caused the same improvement on photobleaching as 10 mM AA on Alexa 488 and Cy3.[43] Also for Atto 565 a few μM NPG allowed reaching the plateau; TX and AA required concentrations were lower (≈50 μM) than for Atto 488.

We then tested the effects of combinations of different reagents (**Figure 7**). We first fixed NPG concentration (at 2 μM) and compared the effects of mixing it with AA, TX and a

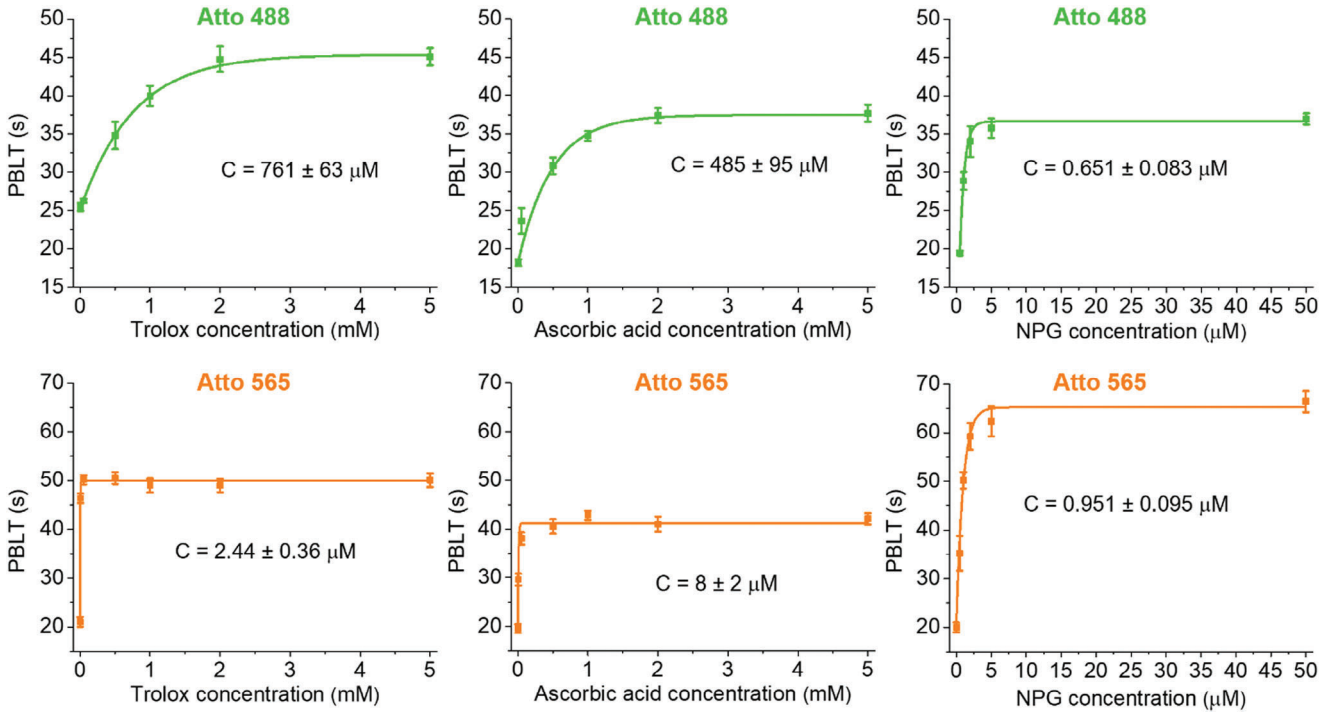

Figure 6. Effects of different reagents on photobleaching. Photobleaching lifetimes (PBLTs) of Atto 488 (top, green) and Atto 565 (bottom, orange) in the presence of different concentrations of Trolox, Ascorbic Acid and n-propyl gallate (NPG). Each lifetime value was obtained by fitting the temporal decay of intensity observed in those conditions (see Figure S6, Supporting Information and Supplementary Methods). PBLTs versus reagent concentrations were here fitted with a monoexponential function $y = A \exp(-x/C) + y_0$. Obtained C values are reported on each graph. Lifetime data were acquired in TIRFm from 10–30 different fields of view from samples of 2–4 independent repetitions. Results are mean ± standard error of the mean (SEM).

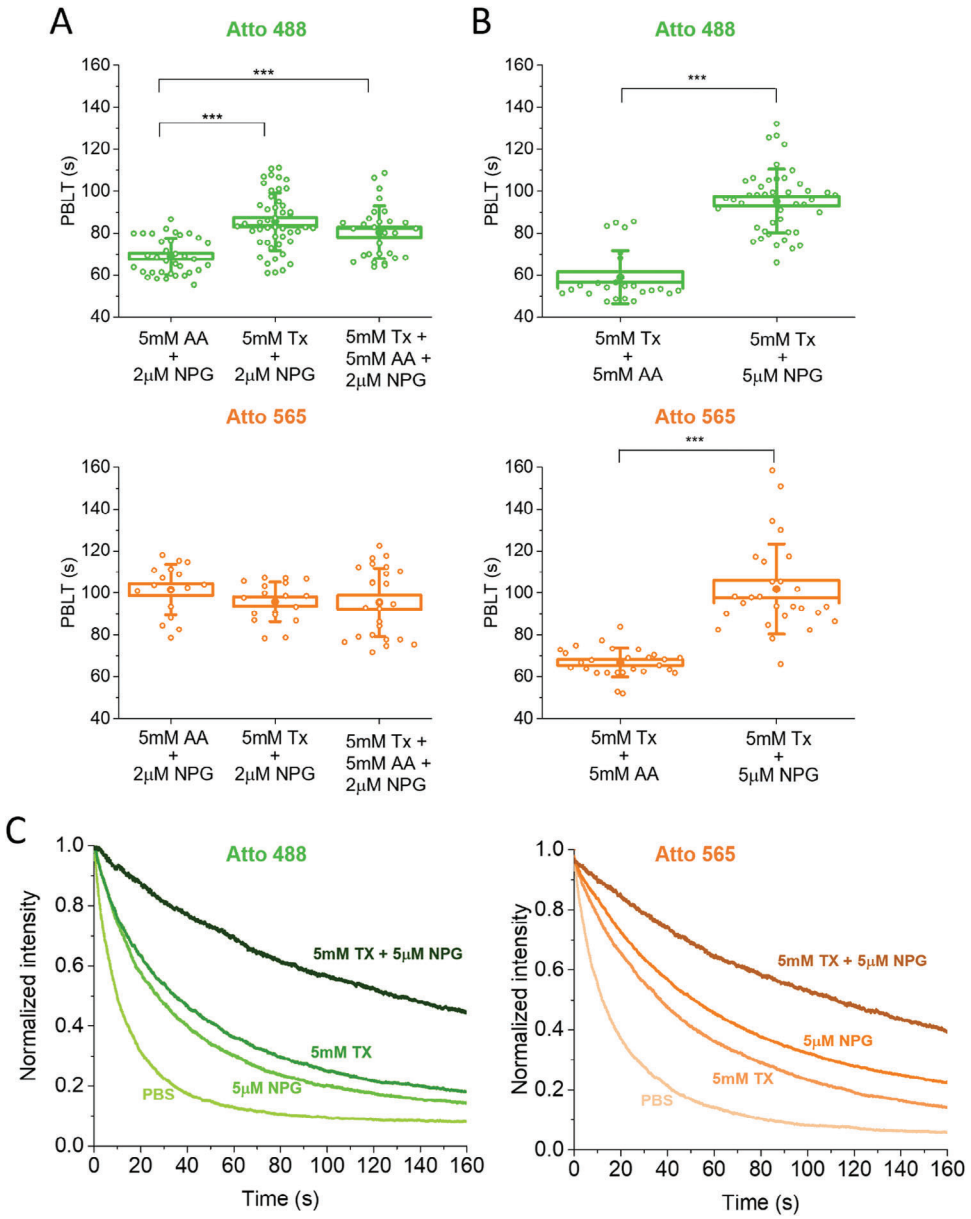

Figure 7. Reduction of photobleaching with mixed reagents. A) Atto 488 (top, green) and Atto 565 (bottom, orange) photobleaching lifetimes (PBLTs) observed adding a mixture of ascorbic acid (AA), Trolox (TX) or both with a fixed concentration of n-propyl gallate (NPG). ***$P < 0.001$, 1-way ANOVA, Bonferroni multiple comparisons. Box: standard error of the mean (SEM); whisker: SD; dots: individual fields of view, from 2–4 independent repetitions. B) As in A, for a mixture of TX and AA and a mixture of TX and NPG. ***$P < 0.001$, Student's test. C) Examples of temporal decay of intensity observed in TIRF under different medium compositions for Atto 488 (left, green) and Atto 565 (right, orange).

combination of TX and AA (by using 5 mM for both TX and AA, where their plateaus were already reached for both dyes) (Figure 7A). On Atto 488, we measured a longer PBLT with a mix of TX and NPG than with AA and NPG; we did not find further improvement by using the three reagents together. For Atto 565, we did not find significant differences between the three situations. We discarded therefore the combination of NPG with AA and of the three reagents together and compared a mix of TX plus AA with a mix of TX plus NPG (by fixing TX concentration at 5 mM and using 5 mM for AA and 5 μM for NPG, concentrations at which the plateaus were already reached); for both dyes, we observed a significantly longer PBLT when using the combination of TX and NPG (Figure 7B). The comparisons reported in Figure S11 (Supporting Information) show that using 5 μM NPG is significantly better than using 2 μM NPG, at least for Atto 488 (and it is not worse for Atto 561).

These data indicated that in all cases and for both dyes, the observed PBLTs were higher with mixed reagents than with single reagents at their plateau, likely thanks to a simultaneous suppression of different bleaching pathways; importantly, the best combination found (TX plus NPG) was the most effective for both dyes (Figure 7). A recent study that searched for the best

photobleaching conditions on different dyes by comparing TX, ROXS or deoxygenation plus ROXS, on Atto 488 obtained a final improvement in PBLT of 4.4 times (Atto 565 was not considered in the study).[27] Here, on Atto 488 we achieved an improvement of ≈6 times (14 to 95 ms) with the combination of TX+NPG. Another work considered Atto 565 comparing: oxygen depletion plus AA or MV (methyl viologen) or ROXS (based on AA plus MV), TX plus MV, TX alone; the authors could not find a solution significantly better than TX alone.[37] Here we showed that a better solution is its combination with AA and especially with NPG.

2.7. Two-Color Single-Particle Tracking on Fast Diffusing p75^{NTR} Receptor

The examined improvements are particularly important to study interactions of single fast-moving molecules. In order to test if the best-identified experimental conditions determined above are sufficient, we performed simultaneous two-color single-particle tracking on the p75^{NTR} membrane receptor in living cells. We used labelling through Sfp phosphopantetheinyl transferase (Sfp): this strategy allows a covalent conjugation of the dye to a serine residue of a peptide tag inserted in the receptor sequence resulting in a controlled 1:1 stoichiometry between dye and receptor.[44,45] We used S6-tagged p75^{NTR}, as previously used in single-color SPT studies on this molecule.[7,46]

We used the best conditions for collar position and immersion oil for each cover glass materials: 0.17 collar position and Leica oil for D263M; 0.19 collar position and Nikon oil for N-PK51. First, we performed single-color experiments on SK-N-BE (2) cells cultured in petri dishes for microscopy with thin bottom cover glass made of standard D263M and of N-PK51 materials. We labelled the receptors with Atto 565. We confirmed that experiments on living cells using the new type of cover glass are feasible. We compared the distribution of the short-time diffusion coefficient D_{12}[47] in the two cases and we obtained the same results on the two cover glasses (Figure S12, Supporting Information, peak values: 0.53 ± 0.01 μm^2/s). We then performed simultaneous two-color SPT by labelling p75^{NTR} receptors with a mixture of Atto 565 and Atto 488. First, we carried out the experiment on D263M cover glass (**Figure 8**A; Videos S1–S3, Supporting Information). We measured the D_{12} distribution, and observed that in the two-color configuration only the 565-channel produced results comparable with the single-color experiment while the 488-channel produced a distribution entirely shifted toward higher diffusivities (with peak values of 0.52 ± 0.02 and 0.69 ± 0.02 μm^2/s for 565 and 488 channels respectively, Figure 8). We also performed the two color SPT experiment with a different receptor, i.e., TrkA, and also in this case, we observed a shift toward higher D for its distribution when estimated on the 488-channel, compared to the 565-channel (Figure S13, Supporting Information). We then performed two-color SPT on p75^{NTR} receptors using N-PK51 cover glasses (Figure 8B; Videos S4–S6, Supporting Information). In this case, we obtained the same distribution of D_{12} in both the 565 and 488 channels (with peak values of 0.52 ± 0.02 μm^2/s for both channels), comparable with that obtained in the single-color case. Thus, the shift for the 488-channel observed using the D263M cover glass was likely due to the low SNR in that channel, which causes significant tracking errors due to high percentages of missed detections. To confirm this hypothesis, we simulated movies of single molecules diffusing with a diffusivity of 0.55 μm^2/s, mimicking conditions (signal intensity, background, noise) similar to those observed in experiments on D263M cover glass (Figure S14, Supporting Information); we then performed the SPT analysis on the simulated movies. We observed the same shift of the diffusivity histogram peak for the situation corresponding to the 488 channel (Figure S14, Supporting Information). Experimental distributions for the 565-channel case are broader compared to the simulated ones, most probably because of the highly complex and heterogeneous environment of the cell membrane (such as areas with different compositions, interactions with membrane structures and other molecules) that cause an intrinsic spread in diffusivities. On the other side, the distribution width obtained using the 488 channel appears dominated by tracking errors and thus is similar between experimental and simulated movies. The impact of immobile dyes causes a shoulder in the left tail of the experimental distributions, which is higher for Atto 565 than for Atto 488; this difference is caused by a higher non-specific adhesion for the first dye, as observable in our results and reported in the literature.[48,49]

In conclusion, with standard cover glasses it was not possible to obtain reliable results in both channels in two-color SPT even when minimizing the autofluorescence of medium, cells and oil. The challenge was overcome by using the N-PK51 cover glasses, which yielded higher SNR in the 488-channel and reliable results in two-color SPTs, even with fast receptors such as p75^{NTR}.

3. Discussion

The development of ever more sensitive single-molecule microscopy applications requires continuous efforts to overcome limitations imposed by the experimental setups, from microscopy components to fluorescent probes.[50–52] In this work, we addressed two essential requirements for quantitative single-molecule imaging and tracking, i.e., signal-to-noise ratio and photostability, achieving a simultaneous two-color TIRFm configuration able to visualize fast-diffusing membrane receptors labelled with minimally-invasive dyes in living cells.

Reaching this goal required understanding and dealing with different background sources within the setup, which significantly affect the SNR of single molecules. In particular, we demonstrated that multicolor applications are mostly hindered by the background resulting from the cover glass, whose standard material is borosilicate glass (see also Supplementary discussion). Its emission in red and far-red regions under excitation at shorter wavelengths strongly limits the use of those spectral bands for detecting single molecules in multicolor configurations. We searched for different possible materials to be used as cover glasses in TIRFm systems that, especially considering commercial ones, have strict requirements on the properties of the cover glass, i.e., thickness of 0.17 mm and refractive index of 1.52. This hinders the use of quartz and fused silica which have much lower autofluorescence than glass[53,54] but a refractive index of 1.46 that causes aberrations in setups designed for a 1.52 value. After extensive searching, we selected Schott N-PK51 glass for making custom cover glasses (See Note S1 and Figure S2, Supporting Information). Our tests showed a significantly

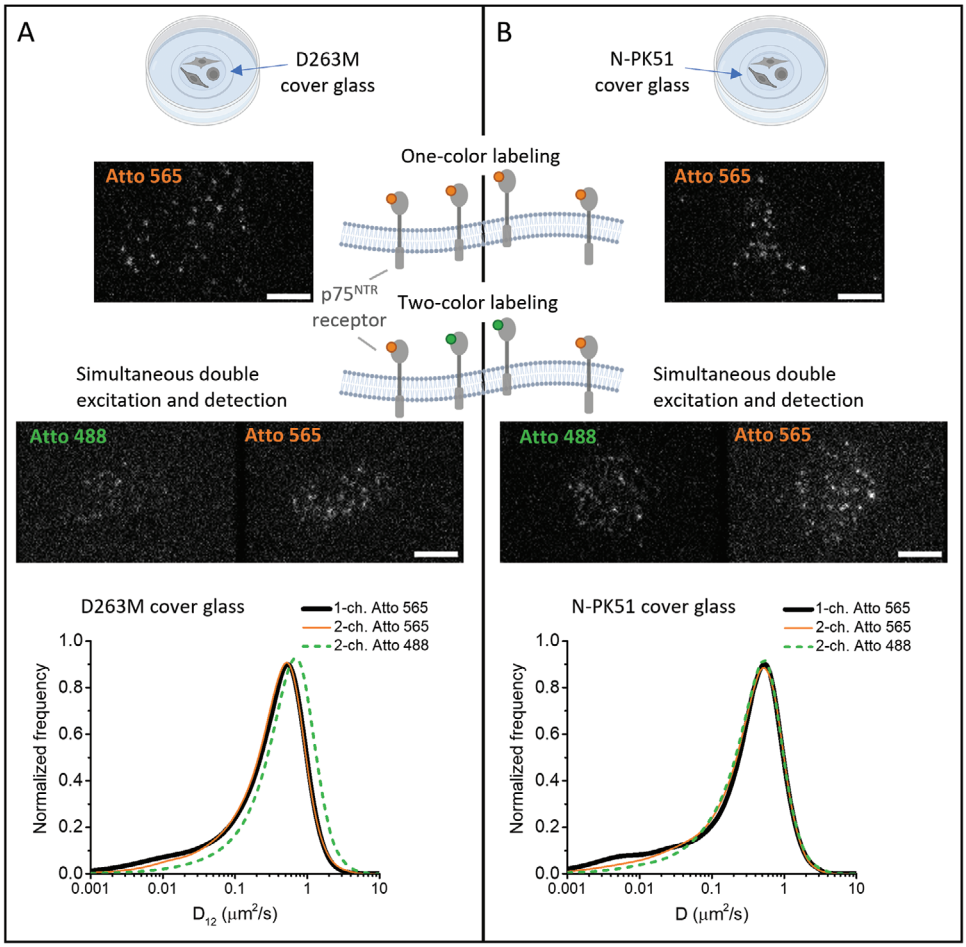

Figure 8. Single particle tracking of p75^{NTR} receptors. One-color and two-color SPT were performed on SK-N-BE cells grown on D263M (A) and N-PK51 (B) cover glasses. p75^{NTR} receptors were labeled with Atto 565 for one-color experiments or with a mix of Atto 565 and Atto 488 for two-color experiments. TIRFm representative images from the acquired movies are shown (scale bar: 5 μm). On the bottom: distributions of short-time diffusion coefficients (D_{12}) extracted with single particle tracking analysis on one-color acquisitions (1-ch. Atto 565, thick black curves), simultaneous two-color acquisitions (2-ch.; thin orange curves for Atto 565 and dashed green curves for Atto 488). D263M cover glass, 1-ch Atto 565: 4086 tracks. D263M cover glass, 2-ch Atto 565: 2501 tracks. D263M cover glass, 2-ch Atto 488: 2119 tracks. N-PK51 cover glass, 1-ch Atto 565: 2127 tracks. N-PK51 cover glass, 2-ch Atto 565: 1828 tracks. N-PK51 cover glass, 2-ch Atto 488: 2086 tracks. Trajectories were obtained from 6–8 different cells from two independent repetitions in each case. Partly made with BioRender.com.

reduced autofluorescence in the green region under 488 nm excitation compared to standard cover glasses. As a consequence of this, the material allowed a significant improvement of the SNR for simultaneous two-channel imaging based on "488" and "565" dyes, which we identified as the best couple for this kind of experiments. The slightly different optical properties of N-PK51 compared to the standard material can be addressed even in a commercial system, thanks to small corrections introduced by the objective collar and the immersion oil.

For live-cell experiments, two other background sources were considered, namely cells and cell medium. Most cell autofluorescence is excited at wavelengths below 450 nm.[21,55] However, in various cell types, the 488 nm wavelength excites flavins which emit in the range 500–650 nm with a peak at ≈550 nm.[34,56] The emission in orange and red regions excited at 561 or 635 nm can instead be associated with porphyrins.[57] The latter have a main absorption peak ≈400 nm (Soret band) plus minor bands between 500 and 700 nm (Q bands) and emit in the orange-red region (between 600 and 700 nm).[56,58] Since this fluorescence emission is usually lower than the one excited at 488 nm, single-color fluorescence measurements are often performed using far-red-emitting dyes.[59] However, we demonstrated that by selecting suitable TIRFm penetration depths for SPT on the cell membrane, the contribution of cells to the background can be less than 2% under 488 nm excitation (only 1% higher compared to the single-channel 635-case) when using the standard D263M glass; using the proposed N-PK51 cover glass, where the background without cell is ≈40% than for D263M, the contribution of cells to the background is expected to be not higher than 5% upon excitation at 488 nm (and even lower for excitation at 561 nm). Furthermore, we identified a cell medium (FluoroBrite DMEM) that allowed us to reduce background emissions to levels comparable with those of PBS; this medium ensures cell health and avoids the use of saline buffers alone, which lack essential elements for cells. Thus, we could confirm that the most limiting factor for TIRFm-based multicolor single-molecule imaging is the

background from the cover glass, and its emission is the main one to consider in the choice of the channels, at least when those of cells and cell medium are properly minimized. For these reasons, we can confirm the selection of the 488–565 dye pair as suitable also for TIRFm on living cells.

Especially when using small and minimally invasive organic dyes another crucial issue in quantitative single-molecule microscopy is photobleaching, which limits the number of photons emitted before photodestruction of the marker.[12] Studies on photobleaching revealed the complexity of the phenomenon, still poorly understood and stemming from different, dye-dependent mechanisms, including interactions with reactive oxygen species (ROS), and reactions of excited states (especially triplet ones) of the dye.[26,35] Several methods were used to reduce photobleaching, from deoxygenation to the addition of triplet state quenchers or reducing and oxidizing reagents.[60] We focused on methods known to be compatible with living cells, and in particular on three reagents with potential antibleaching properties: Trolox (TX, a free radical scavenger, an antioxidant and possibly a triplet state quencher), ascorbic acid (AA, a well-known antioxidant with a possible scavenging activity toward some free radicals) and n-propyl gallate (NPG, antioxidant and scavenger for some ROS).[35,36,60,61] In general, the action of each reagent and the best solution against photobleaching strongly depend on the dye being considered: some strategies effective on some dyes may not be effective or have adverse effects on others.[27,37,40] For this reason, multicolor studies have the additional challenge of finding a solution that works well for multiple dyes simultaneously. We achieved this objective on the two dyes of interest Atto 488 and Atto 565. Both showed less photobleaching when adding TX, AA or NPG. For both dyes we found the most effective solution with a combination of TX and NPG.

We applied the developed tools to perform two-color SPT experiments in live cells. We selected the labelling based on Sfp phosphopantetheinyl transferase as this minimizes perturbations thanks to a controlled 1:1 stoichiometry between dye and receptor and the insertion of only a very short tag (12 residues) in the protein sequence.[44–46] We performed two-color imaging on $p75^{NTR}$ receptors labeled with two small organic dyes. This choice was driven by the observed alteration of its dynamics upon labeling with Qdots with respect to small organic dyes.[7] More importantly, this is a particularly fast receptor and, as we also showed here, higher diffusivities create worse SNR conditions. We demonstrated that the presented methods allow reliable single-molecule tracking simultaneously in two channels even on challenging receptors, unlike standard cover glasses, effectively extending the potential of TIRFm-based SPT.

4. Conclusion

In summary, our study provides a series of strategies to achieve single-molecule tracking in two colors by TIRFm in living cells, and in particular for minimizing background and photobleaching. We demonstrated a case where these optimizations have been necessary to obtain compatible results in two different channels, verifying by simulation that the source of the mismatch was a too low SNR in one of them. One of the main observations here reported is the fact that the highest unavoidable impact on the background comes from the optical glass on which the sample is placed, while we presented strategies to minimize the impact of oil, medium, and cell autofluorescence. We selected and tested a new optical material to be used as cover glass, and developed strategies to correct the aberrations worsened by its introduction in our setup; this allowed a significant reduction of background noise with respect to the case of standard cover glasses. Further investigations in this direction can identify solutions for increasingly advanced applications, e.g. decreasing the background in three and more channels.

Several studies pointed out the importance of knowing the origin of materials' luminescence to control and modulate it, especially in bioimaging.[62–64] Some applications (e.g., when the material itself is used as probe) require the enhancement of these emissions and have been investigated more [62–64]; but, at the same time, some optical imaging methods, as the case examined here, are still challenged by these emissions arising from optical components of the setup and require lowering them for increasing imaging sensitivity. Unfortunately, too few data on this issue are present in the literature or available from commercial companies; we hope that this work will stimulate more research on the fluorescence characteristics of different glasses, increasing the demand for cover glasses with reduced autofluorescence, promoting therefore their accessibility.

5. Experimental Section

Microscopy Setup: Microscopy experiments were carried out with a Leica DM6000 inverted microscope (Leica Microsystems) equipped with an epifluorescence module, DIC in transmission, TIRF-AM module, HCX PL APO 100.0X oil-immersion objective (NA 1.47), EM-CCD camera (iXon Ultra 897, Andor), four laser lines (405, 488, 561, and 635 nm), incubator chamber to maintain 37 °C and 5% CO_2 conditions for live cell imaging. Leica type F immersion oil was used unless otherwise specified. An external laser combiner (iFLEX-adder, QiOptiq) with kineFLEX polarization maintaining fibers (QiOptiq) and kineMATIX fiber coupler (QiOptiq) was used with a 488 nm supplementary laser (iFLEX-iRIS, Qioptiq) for simultaneous two-color excitation. The power of the additional 488 nm laser was tuned by a DAC. To detect two channels at the same time, a Dual View (Optical Insights DV-CC) was placed in front of the EM-CCD camera, so that emitted light was split and collected in the two halves of the camera. An Optomask adjustable field mask (OPTMSK-L, Andor) was included between the microscope output and the Dual View to limit the illuminated area of the camera and increase the frame rate. The fluorescence cube Leica Quad ET TIRF MC was used for Laser line 405/488/561/635 nm No 11 523 026 (except when differently stated). In the Dual View, two alternative filter sets were used: i) dichroic beam splitter T600lpxr, with filters Chroma ET525-50 and r647lp, for detection of green-emitting dyes and far-red-emitting dyes respectively; ii) dichroic beam splitter 565dcxr, with filters Chroma ET525-50 and Semrock FF01-600/52, for detection of green-emitting dyes and orange-emitting dyes respectively. For single-color comparisons between Atto 565 and Abberior STAR 635p the Cy3 and Cy5 cube were also used as specified in the SNR measurements section.

EM-CCD parameters were set to: temperature −75 °C, pixel clocking rate 17 000 MHz, vertical shift speed 0.5 µs, vertical clock voltage +2, EM gain 1000; acquisitions were performed under frame-transfer mode and the readout time was typically 16 ms.[7,65]

SNR Measurements: Signal-to-noise ratio (SNR) was measured on fluorophores adhered to the bottom of WillCo dishes with their original D 263 M cover glass or with custom cover glasses made of Schott N-PK51 glass (Figures 1B,D, 2B–D, and 3E; Figure S4, Supporting Information). The latter cover glasses were manufactured by CLaser Photonics, Inc. (CLASER), using the glass purchased from Schott. SNR measurements were also performed on fluorophores that labeled membrane receptors TrkA and

$p75^{NTR}$ in living cells (Figure 1B; Figure S1, Supporting Information, see also Supplementary Methods).

In all cases, samples were prepared with fluorophore densities low enough to distinguish single molecules. For measurements on adhered fluorophores, a solution of them in PBS (typical concentration of ≈1 nM) was deposited on the cover glass for ≈10 min. After extensive washing to remove fluorophores remained in suspension or weakly adhering, the dish was filled with PBS and the sample was immediately observed with TIRFm.

For single-color comparisons between Atto 565 and Abberior STAR 635p (Figure 1B), 561 nm excitation was used with a Cy3 cube and 635 nm excitation with a Cy5 cube, respectively, with both lasers power set to 3 mW at the objective. For single- or double-color measurements on Alexa 488 and Atto 565, single or double excitation was used at 488 (3.5 mW) and 561 nm (3 mW), with cube and filters as specified in the Microscopy setup section.

For preliminary evaluations of the SNR achievable in two-color configurations with different pairs of channels (without needing setups for simultaneous excitation and detection for all possible pairs), the Dual View system was exploited detailed above considering one window at a time under single excitations. Single-color acquisitions was performed on fluorophores for each one of the considered channels; then, for each possible pair of channels, the background resulting upon excitation was measured at the shorter wavelength in the longer wavelength detection channel. After subtracting the offset, this background was added to the images acquired under the single excitation. This allowed to estimate the SNR of the channel at longer wavelengths upon double excitations. In this way, three couples of channels were compared with excitations at 488 + 561, 561 + 635, and 488 + 635 nm excitation (Figure 1D).

Hundred-frame time series were acquired with 40 ms integration time in different fields of view for each sample.

The SNR was calculated as $(S - B)/\sigma$, where S is the single molecule intensity included background contribution, B is the background intensity, σ is the background standard deviation. TrackMate 6.0.1 plugin in ImageJ was exploited to estimate S.[66] Single molecule detection was performed by using the LoG detector (Laplacian of Gaussian filter) with optimized blob diameter of 0.3 micron, checking "pre-process with median filter" and "sub-pixel localization" options. A "quality threshold" was applied, whose value was optimized checking detection results (typically ≈1000); in the following detection step, filtering on mean intensity contributed to limit spurious detections. On the detected spots, tracking was performed by using the Simple LAP tracker algorithm, and then spots in tracks lasting at least four frames were considered to exclude false detections. For measurements in live cells, filters were also applied on the displacement and velocity of tracks to select only dyes labelling moving receptors and exclude the ones non-specifically adhered to the glass. For each analyzed movie, TrackMate allowed to extract the mean intensity for each spot included in the reconstructed tracks. The average of these intensities corresponds to S. Then the background B was measured with its standard deviation σ for each movie selecting a region of interest (ROI) in a dye-free area (note that, when reporting the B value alone, the offset is subtracted; see Experimental Section). Using ImageJ, the intensity mean and standard deviation within the ROI was extracted and averaged these quantities over time on the whole movie to obtain the final value of B and σ. For in-cell evaluation, the background was evaluated in areas with non-transfected cells.

Single-Particle Tracking: SH-SY5Y and SK-N-BE cells were transfected with S6-p75 or S6-TrkA, then labelled with Coenzyme A (CoA)-dyes as described in the Supplementary Methods and discussed in.[44,67] After labelling, they were immediately imaged by TIRFm. A constant ROI was selected containing cell basal membrane; ROI were 318 × 236 pixels (50.88 × 37.76 µm, pixel size 0.16 µm) for two-channel acquisitions and 159 × 236 pixels for one-channel acquisitions. Two hundred fifty-frame time series were acquired with an integration time of 40 ms, corresponding to a frame time of 56 ms. Penetration depth was set to 110 nm for the 561 nm internal excitation, corresponding to a depth of ≈96 nm for the 488 nm external one in the case of a simultaneous two-color acquisition.

For the tracking analysis, some pre-processing steps were first performed with the ImageJ software: i) in the case of two-channel acquisition, the movie was split into two movies, one for each channel; ii) for each movie a maximum intensity projection was created to identify the contours of the cell membrane; iii) a mask was applied to the movie using the identified contours to exclude the spots outside the cell due to the fluorophores adhered in a non-specific way to the cover glass, analogously as in.[7,47] The masked movies were then processed with u-track software version 2.2.1[68] in MATLAB to obtain single-particle trajectories.

For the calculation of distribution coefficients (Figure 8; Figures S1 and S12–S14, Supporting Information), tracks were selected including at least 6 detected spots and lasting at least 9 frames in total (including gaps). Subtrajectories created by merge and split events, was divided as described in.[7] On the obtained subtrajectories, the short-time diffusion coefficient D_{12} was calculated from the first two points of the Mean Square Displacement (MSD) function.[7,47,69] The D_{12} distributions were determined considering uncertainties on D_{12} and weighting each trajectory with the number of frames where its spots were detected, as in.[47] Distribution integrals were normalized to 1.

More details on Experimental Section are reported in the Supplementary Methods (synthesis of CoA-fluorophores, production of Sfp, cell culture, receptors expression and labelling, measurements and analysis descriptions, simulations implementation).

Supporting Information

Supporting Information is available from the Wiley Online Library or from the author.

Acknowledgements

The authors acknowledge Laura Marchetti and Fulvio Bonsignore for developing the initial versions of some of the constructs used in this work. The authors acknowledge Filippo Fabbri for measurements with the Renishaw micro-Raman system. This research received funding from Scuola Normale Superiore (SNS16C_B_LUIN, SNS_RB_LUIN, SNS19_A_LUIN), from Fondazione Pisa (project Nanotechnology for tumor molecular fingerprinting and early diagnosis, RST 148/16), and from the European Union Next-GenerationEU through the PIANO NAZIONALE DI RIPRESA E RESILIENZA (PNRR – MISSIONE 4 COMPONENTE 2) within the National Quantum Science and Technology Institute (NQSTI – INVESTIMENTO 1.3; PE_00000023) and the Tuscany Health Ecosystem (THE – INVESTIMENTO 1.5; ECS_00000017). The graphical abstract was partly made with bioRrender.com.

Conflict of Interest

The authors declare no conflict of interest.

Author Contributions

C.S.S. performed conceptualization, methodology, software, validation, formal analysis, investigation, and data curation; wrote the original draft; wrote, reviewed, and edited the draft; and visualization. A.M. and R.A. performed methodology and wrote, reviewed, and edited the draft. F.B. provided resources; wrote, reviewed, and edited the draft; and provided supervision and funding acquisition. S.L. performed conceptualization, methodology, software; wrote the original draft; wrote, reviewed, and edited the draft; and provided visualization, project administration, supervision, funding acquisition, and resources.

Data Availability Statement

The data that support the findings of this study are available from the corresponding author upon reasonable request.

Keywords

cover glasses for TIRF microscopy, live cell nanoscopy, multicolor single molecule imaging, optical glass fluorescence, photobleaching reduction

Received: August 17, 2023
Revised: October 14, 2023
Published online:

[1] T. C. Rao, T. J. Nawara, A. L. Mattheyses, in *Cell Polarity Signaling. Methods in Molecular Biology*, (Eds.: C. Chang, J. Wang), Humana Press Inc., New York **2022**, pp. 45.
[2] A. E. Ward, V. Kiessling, O. Pornillos, J. M. White, B. K. Ganser-Pornillos, L. K. Tamm, *J. Biol. Chem.* **2020**, *295*, 15183.
[3] M. Midorikawa, *Neurosci. Res.* **2018**, *136*, 1.
[4] A. Kusumi, T. A. Tsunoyama, K. M. Hirosawa, R. S. Kasai, T. K. Fujiwara, *Nat. Chem. Biol.* **2014**, *10*, 524.
[5] R. S. Kasai, A. Kusumi, *Curr. Opin. Cell Biol.* **2014**, *27*, 78.
[6] A. Kusumi, T. K. Fujiwara, R. Chadda, M. Xie, T. A. Tsunoyama, Z. Kalay, R. S. Kasai, K. G. N. Suzuki, *Annu. Rev. Cell Dev. Biol.* **2012**, *28*, 215.
[7] L. Marchetti, F. Bonsignore, F. Gobbo, R. Amodeo, M. Calvello, A. Jacob, G. Signore, C. Schirripa Spagnolo, D. Porciani, M. Mainardi, F. Beltram, S. Luin, A. Cattaneo, *Proc. Natl. Acad. Sci. USA* **2019**, *116*, 21563.
[8] R. S. Kasai, K. G. N. Suzuki, E. R. Prossnitz, I. Koyama-Honda, C. Nakada, T. K. Fujiwara, A. Kusumi, *J. Cell Biol.* **2011**, *192*, 463.
[9] B. Da Rocha-Azevedo, S. Lee, A. Dasgupta, A. R. Vega, L. R. De Oliveira, T. Kim, M. Kittisopikul, Z. A. Malik, K. Jaqaman, *Cell Rep.* **2020**, *32*, 108187.
[10] U. Resch-Genger, M. Grabolle, S. Cavaliere-Jaricot, R. Nitschke, T. Nann, *Nat. Methods* **2008**, *5*, 763.
[11] C. Schirripa Spagnolo, S. Luin, *Int. J. Mol. Sci.* **2022**, *23*, 14949.
[12] P. Reineck, A. Francis, A. Orth, D. W. M.o Lau, R. D. V. Nixon-Luke, I. D. Rastogi, W. A. W. Razali, N. M. Cordina, L. M. Parker, V. K. A. Sreenivasan, L. J. Brown, B. C. Gibson, *Adv. Opt. Mater.* **2016**, *4*, 1549.
[13] Z. Wang, X. Wang, Y. Zhang, W. Xu, X. Han, *Small* **2021**, *17*, 2005133.
[14] L. Abraham, H. Y. Lu, R. C. Falcão, J. Scurll, T. Jou, B. Irwin, R. Tafteh, M. R. Gold, D. Coombs, *Sci. Rep.* **2017**, *7*, 11379.
[15] C. Schirripa Spagnolo, A. Moscardini, R. Amodeo, F. Beltram, S. Luin, *BMC Biol.* **2023**, *21*, 190.
[16] J. Morise, K. G. N. Suzuki, A. Kitagawa, Y. Wakazono, K. Takamiya, T. A. Tsunoyama, Y. L. Nemoto, H. Takematsu, A. Kusumi, S. Oka, *Nat. Commun.* **2019**, *10*, 5245.
[17] A. N. Trukhin, *J. Non. Cryst. Solids* **2011**, *357*, 1931.
[18] H. Yang, Z. Zhu, *J. Lumin.* **2021**, *231*, 117804.
[19] K. Saito, A. J. Ikushima, *Phys. Rev. B: Condens. Matter Mater. Phys.* **2000**, *62*, 8584.
[20] Andersson, Baechi, Hoechl, Richter, *J. Microsc.* **1998**, *191*, 1.
[21] Y. Kumamoto, A. Taguchi, S. Kawata, *Adv. Opt. Mater.* **2019**, *7*, 1801099.
[22] X. Lu, Y. Zhang, H. Gross, *Appl. Opt.* **2019**, *58*, 7404.
[23] X. Lu, O. Rodenko, Y. Zhang, H. Gross, *Appl. Opt.* **2019**, *58*, 3589.
[24] Y. Gambin, V. Vandelinder, A. C. M. Ferreon, E. A. Lemke, A. Groisman, A. A. Deniz, *Nat. Methods* **2011**, *8*, 239.
[25] T. Ensslen, J. C. Behrends, *Lab Chip* **2022**, *22*, 2902.
[26] A. P. Demchenko, *Methods Appl. Fluoresc.* **2020**, *8*, 022001.
[27] T. A. Tsunoyama, Y. Watanabe, J. Goto, K. Naito, R. S. Kasai, K. G. N. Suzuki, T. K. Fujiwara, A. Kusumi, *Nat. Chem. Biol.* **2018**, *14*, 497.
[28] N. Li, R. Zhao, Y. Sun, Z.i Ye, K. He, X. Fang, *Natl. Sci. Rev.* **2017**, *4*, 739.
[29] J. E. Aubin, *J. Histochem. Cytochem.* **1979**, *27*, 36.
[30] L. Wasim, B. Treanor, in *B Cell Receptor Signaling*. (Ed: C. Liu),Humana Press Inc., New York **2018**, pp. 183–192.
[31] M. Zabolocki, K. Mccormack, M. Van Den Hurk, B. Milky, A. P. Shoubridge, R. Adams, J. Tran, A. Mahadevan-Jansen, P. Reineck, J. Thomas, M. R. Hutchinson, C. K. H. Mak, A. Añonuevo, L. H. Chew, A. J. Hirst, V. M. Lee, E. Knock, C. Bardy, *Nat. Commun.* **2020**, *11*, 5550.
[32] V. A. Spencer, S. Kumar, B. Paszkiet, J. Fein, J. F. Zmuda, *Genet. Eng. Biotechnol. News* **2014**, *34*, 16.
[33] Y. Zhang, P. Sukthankar, J. M. Tomich, G. W. Conrad, *Invest. Ophthalmol. Visual Sci.* **2012**, *53*, 2620.
[34] R. C. Benson, R. A. Meyer, M. E. Zaruba, G. M. Mckhann, *J. Histochem. Cytochem.* **1979**, *27*, 44.
[35] J. Widengren, A. Chmyrov, C. Eggeling, P.-Å. Löfdahl, C. A. M. Seidel, *J. Phys. Chem. A* **2007**, *111*, 429.
[36] T. Cordes, J. Vogelsang, P. Tinnefeld, *J. Am. Chem. Soc.* **2009**, *131*, 5018.
[37] J. Vogelsang, R. Kasper, C. Steinhauer, B. Person, M. Heilemann, M. Sauer, P. Tinnefeld, *Angew. Chem., Int. Ed.* **2008**, *47*, 5465.
[38] T. Ha, P. Tinnefeld, *Annu. Rev. Phys. Chem.* **2012**, *63*, 595.
[39] T. Cordes, A. Maiser, C. Steinhauer, L. Schermelleh, P. Tinnefeld, *Phys. Chem. Chem. Phys.* **2011**, *13*, 6699.
[40] I. Rasnik, S. A. Mckinney, T. Ha, *Nat. Methods* **2006**, *3*, 891.
[41] P. S. Dittrich, P. Schwille, *Appl. Phys. B* **2001**, *73*, 829.
[42] A. K. Gaigalas, L. Wang, K. D. Cole, E. Humphries, *J. Phys. Chem. A* **2004**, *108*, 4378.
[43] C. E. Aitken, R. A. Marshall, J. D. Puglisi, *Biophys. J.* **2008**, *94*, 1826.
[44] L. Marchetti, T. De Nadai, F. Bonsignore, M. Calvello, G. Signore, A. Viegi, F. Beltram, S. Luin, A. Cattaneo, *PLoS One* **2014**, *9*, 113708.
[45] J. Yin, P. D. Straight, S. M. Mcloughlin, Z. Zhou, A. J. Lin, D. E. Golan, N. L. Kelleher, R. Kolter, C. T. Walsh, *Proc. Natl. Acad. Sci. USA* **2005**, *102*, 15815.
[46] L. Marchetti, F. Bonsignore, R. Amodeo, C. Schirripa Spagnolo, A. Moscardini, F. Gobbo, A. Cattaneo, F. Beltram, S. Luin, in *Single Molecule Spectroscopy and Superresolution Imaging XIV*, (Eds.: I. Gregor, R. Erdmann, F. Koberling), SPIE, Single Molecule Spectroscopy and Superresolution Imaging, Bellingham Washington **2021**, p. 20.
[47] L. Marchetti, A. Callegari, S. Luin, G. Signore, A. Viegi, F. Beltram, A. Cattaneo, *J. Cell Sci.* **2013**, *126*, 4445.
[48] L. D. Hughes, R. J. Rawle, S. G. Boxer, *PLoS One* **2014**, *9*, 87649.
[49] Z. Zhang, D. Yomo, C. Gradinaru, *Biochim. Biophys. Acta – Biomembr.* **2017**, *1859*, 1242.
[50] R. B. Quast, E. Margeat, *Nat. Methods* **2021**, *18*, 344.
[51] D. Mahecic, I. Testa, J. Griffié, S. Manley, *Curr. Opin. Chem. Biol.* **2019**, *51*, 84.
[52] K. C. Gwosch, J. K. Pape, F. Balzarotti, P. Hoess, J. Ellenberg, J. Ries, S. W. Hell, *Nat. Methods* **2020**, *17*, 217.
[53] L. M. Davis, B. K. Canfield, X. Li, W. H. Hofmeister, G. Shen, I. P. Lescano-Mendoza, B. W. Bomar, J. P. Wikswo, D. A. Markov, P. C. Samson, C. Daniel, Z. Sikorski, W. N. Robinson, in *Biosensing*, (Eds.: M. Razeghi, H. Mohseni), SPIE, Bellingham, Washington **2008**, p. 70350A.
[54] W. A. W. Razali, V. K. A. Sreenivasan, C. Bradac, M. Connor, E. M. Goldys, A. V. Zvyagin, *J. Biophotonics* **2016**, *9*, 848.
[55] G. A. Wagnieres, W. M. Star, B. C. Wilson, *Photochem. Photobiol.* **1998**, *68*, 603.
[56] A. C. Croce, G. Bottiroli, in *Histochemistry of Single Molecules*, (Eds.: C. Pellicciari, M. Biggiogera), Humana Press Inc., New York **2017**, pp. 15–43.
[57] B. Del Rosal, A. Benayas, *Small Methods* **2018**, *2*, 1800075.
[58] G. Jiang, W. Lei, Y. Hou, X. Wang, *New J. Chem.* **2012**, *36*, 2180.
[59] J. Wu, Z. Shi, L. Zhu, J. Li, X.u Han, M. Xu, S. Hao, Y. Fan, T. Shao, H. Bai, B.o Peng, W. Hu, X. Liu, C. Yao, L. Li, W. Huang, *Adv. Opt. Mater.* **2022**, *10*, 2102514.

[60] W. Gong, P. Das, S. Samanta, J. Xiong, W. Pan, Z. Gu, J. Zhang, J. Qu, Z. Yang, *Chem. Commun.* **2019**, *55*, 8695.
[61] M. E. Alberto, N. Russo, A. Grand, A. Galano, *Phys. Chem. Chem. Phys.* **2013**, *15*, 4642.
[62] K. Zhang, C.-G. Ma, J.-Y. Zhang, B.-M. Liu, Y. Zhou, S.-Q. Guo, J.-Y. Xu, J.-S. Hou, Y.-Z. Fang, L.-R. Zheng, H.-T. Sun, *Adv. Opt. Mater.* **2017**, *5*, 1700448.
[63] P. Jing, D. Han, D.i Li, D. Zhou, L. Zhang, H. Zhang, D. Shen, S. Qu, *Adv. Opt. Mater.* **2017**, *5*, 1601049.
[64] J. Zaumseil, *Adv. Opt. Mater.* **2022**, *10*, 2101576.
[65] C. Schirripa Spagnolo, S. Luin, *Biomol. Concepts* **2023**, *14*, 20220032.
[66] J.-Y. Tinevez, N. Perry, J. Schindelin, G. M. Hoopes, G. D. Reynolds, E. Laplantine, S. Y. Bednarek, S. L. Shorte, K. W. Eliceiri, *Methods* **2017**, *115*, 80.
[67] F. Gobbo, F. Bonsignore, R. Amodeo, A. Cattaneo, L. Marchetti, in *Neurotrophic Factors*, (Ed: S. Skaper), Humana Press Inc., New York **2018**, pp. 295–314.
[68] K. Jaqaman, D. Loerke, M. Mettlen, H. Kuwata, S. Grinstein, S. L. Schmid, G. Danuser, *Nat. Methods* **2008**, *5*, 695.
[69] R. Amodeo, R. Nifosì, C. Giacomelli, C. Ravelli, L. La Rosa, A. Callegari, M. L. Trincavelli, S. Mitola, S. Luin, L. Marchetti, *Biochim. Biophys. Acta – Mol. Cell Res.* **2020**, *1867*, 118614.